Effect of welding heat input and post-welded heat treatment on hardness of stir zone for friction stir-welded 2024-T3 aluminum alloy

Yu CHEN[1], Hua DING[1], Ji-zhong LI[2], Jing-wei ZHAO[3], Ming-jie FU[2], Xiao-hua LI[2]

1. School of Materials and Metallurgy, Northeastern University, Shenyang 110819, China;
2. Beijing Aeronautical Manufacturing Technology Research Institute, Aviation Industry Corporation of China, Beijing 100024, China;
3. School of Mechanical, Materials and Mechatronic Engineering, University of Wollongong, NSW 2522, Australia

Abstract: The microstructure and hardness of the stir zone (SZ) with different welding heat inputs were investigated for friction stir-welded 2024-T3 aluminum by transmission electron microscopy, differential scanning calorimeter and Vickers micro-hardness test. The results show that welding heat input has a significant effect on the hardness of the SZ. Under high welding heat input condition, a higher welding speed is beneficial for improving the hardness of the SZ. However, when the welding heat input is low, the hardness of the SZ elevates with increasing the rotation speed. The hardness of the SZ decreases after post-welded heat treatment due to overaging. The joints welded at 500 r/min and 100 mm/min show a high resistance to overaging. The reduction of hardness in the SZ is only 3.8%, while in other joints, the reduction is more than 10%. The morphology of strengthening precipitates plays important roles for the improvement of hardness.

Key words: aluminum alloy; friction stir welding; heat treatment; heat input; hardness

1 Introduction

Friction stir welding (FSW) has been successfully used in the welding of 2xxx series precipitation-hardened aluminum alloys which are difficult for fusion-welding because of their susceptibility to hot cracking, since this technology was developed in 1991 [1,2]. In FSW, a material experiences intense plastic deformation at elevated temperatures [3−10]. This process leads to a stir zone (SZ) which consists of recrystallized and fine-grained microstructure. This SZ is called dynamic recrystallized zone [11−13]. The fine-grained microstructure is beneficial for obtaining excellent mechanical properties in non-heat-treatable aluminum alloys. In the FSW of 1080 Al alloy, for example, the hardness was significantly increased with the refinement of the microstructure of the SZ [14]. However, soft regions were also reported to form in the FSW of precipitation-hardened aluminum alloys [15,16]. The formation of these soft regions is a sequence of the dissolution or coarsening of strengthening precipitates in

the SZ at elevated welding temperatures. In order to improve the mechanical properties of SZ produced by FSW, many different methods including optimizing the FSW parameters, applying post-welded heat treatment (PWHT), expediting cooling speed, and using submerged FSW, have been explored to minimize the dissolution or coarsening of strengthening precipitates [17,18].

Extensive studies have been performed on PWHT of various Al alloys because of its convenience and efficiency. HU et al [19] reported that the maximum elongation of the PWHT joint was 1.6 times that of the as-welded joints with no loss of tensile strength of a FSW 2024-O aluminum alloy. ELANGOVAN and BALASUBRAMANIAN [20] found that PWHT could enhance the tensile properties of a FSW AA6061 aluminum alloy joint. AYDIN et al [21] reported that the mechanical properties of FSW 2024-T4 aluminum alloys could be significantly improved after a PWHT T6 (190 °C, 10 h) aging treatment. SHARMA et al [22] indicated that PWHT on a 7039 aluminum alloy induced increased elongation at the expense of tensile strength. SULLIVAN and ROBSON [23] conducted a research of

PWHT on an AA7449 aluminum alloy thick plate. They found that the hardness in the SZ was enhanced after PWHT. DANAF et al [24] stated that PWHT could eliminate the negative effect of FSW on the strength and hardness in the SZ of AA6082 aluminum alloy.

Most previous works focus on using PWHT to improve the mechanical properties, but there is a lack of consideration in the variation of mechanical properties of materials in the following utilization. 2xxx series precipitation-hardened aluminum alloys target towards the applications in the aerospace sector. The utilization temperature of this series alloy may be higher than room temperature, and the resistance to overaging is important. Therefore, it is necessary to evaluate the capacity of the resistance to overaging for precipitation-hardened aluminum alloys.

In the current study, FSW was conducted under different welding heat input conditions. The post FSW natural aging (PWNA) condition was obtained and regarded as a PWHT state. All the post-welded heat treatments were carried out under PWNA state. This work aimed at researching the effect of welding heat input and post-PWNA heat treatment (P-PWNA−HT) on the hardness of the SZ. The relationship between welding heat input and the microstructure in SZ will also be discussed.

2 Experimental

2.1 Welding heat input

Welding heat input is one of the most important factors for FSW, and the mechanical properties of SZ under as-welded and PWHT states vary with different welding heat inputs. The welding heat inputs within SZ are very difficult to be measured due to the intense plastic deformation induced by the rotation and the translation of a stirring tool. Based on the heat flow model of HAO et al [5], the welding heat input can be described as

$$q = \frac{4}{3}\pi^2 \mu p \omega R^3 \tag{1}$$

where q is the heat input, μ is the friction coefficient, p is the pressure, ω is the rotation speed and R is the radius of the shoulder. If the welding speed is considered, Eq. (2) is obtained

$$Q = \frac{4}{3}\pi^2 \mu p R^3 \frac{\alpha\omega}{v} \tag{2}$$

where Q is the heat input per length, α is the heat input efficiency, and v is the welding speed. In this work, only one kind of stirring tool is used and the welding condition is the same, α, μ, p and R are assumed to be constant, and only ω and v are variable, so Q can be expressed as

$$Q = \alpha\beta\frac{\omega}{v} \tag{3}$$

where β is a coefficient. Based on the report of FU et al [25], the peak temperature of the SZ can also be used to express the welding heat input as

$$\frac{T}{T_\mathrm{m}} = K(\frac{\omega^2}{10^4 v})^\gamma \tag{4}$$

where T is the peak temperature of SZ during FSW, T_m is the melting point of the alloy, and K and γ are coefficients. γ is reported to range from 0.04 to 0.06, and K is between 0.65 and 0.75. In this work, K and γ are assumed to be constants because of the same welding condition.

From Eqs. (3) and (4), the welding heat input is dependent on the rotation speed and welding speed. Both ω/v (liner energy, LE) and ω^2/v (heat index, HI) are used to quantify the heat input in this work. It should be noticed that LE is mainly affected by the welding speed, while HI is affected by the rotation speed.

2.2 Experimental procedure

2024-T3 aluminum alloy sheets of 3 mm in thickness were used. The nominal chemical compositions of this alloy are listed in Table 1. The sheets were joined by FSW with different welding heat inputs, which were divided into two groups based on the heat inputs (using LE and HI), as shown in Table 2. In FSW, an H13 steel stirring tool consisting of 10 mm diameter shoulder and 4 mm diameter pin was employed. After FSW, the as-welded samples were kept in natural environment for 18 months to obtain a stable PWNA condition. In order to investigate the effect of P-PWNA−HT on the microstructure and the hardness of FSW joints, artificial aging was carried out at 220 °C for a soaking time of 10 h in an electric oven.

Microstructural characterization was performed on the cross-section of plates using a transmission electron microscopy (TEM). Energy-dispersive X-ray spectroscopy (EDXS) analyses were performed using a

Table 1 Nominal chemical composition of studied 2024-T3 aluminum alloy (mass fraction, %)

Cu	Mg	Mn	Fe	Si	Zn	Al
4.22	1.56	0.61	0.18	0.21	0.13	Bal.

Table 2 FSW parameters used in this work and relationship between parameters and heat input

ω/v	HI	LE	Heat input
350/100	1225	3.5	Low
500/100	2500	5	Low
700/100	4900	7	High
500/50	5000	10	High

Tecnai G^{2}20. Vickers micro-hardness test was carried out along the centerlines of the cross-section with a distance between neighboring measured points of 0.5 mm under a load of 50 g for 10 s. Differential scanning calorimeter (DSC) test samples were cut from the stir zone of PWNA and P-PWNA−HT state joints. The DSC sample dimensions were 5 mm in diameter and 0.3 mm in thickness. Samples were heated at a constant heating rate of 10 K/min from room temperature to 550 °C.

3 Results

3.1 Microstructure of stir zone

Figure 1 shows the microstructures of four FSW joints in the SZ at PWNA state. The variation of grain size with welding heat input can be divided into two cases: In the low welding heat input, the grain size increases with increasing the rotation speed of stirring tool (Figs. 1(a) and (b)); and in the high welding heat input, the grain size has obvious growth (Figs. 1(c) and (d)) due to the higher welding heat input. Beside the grain size, the variation of the strengthening precipitates in the SZ with different processing parameters is another important aspect. By comparing the microstructures with low welding heat input (Figs. 1(a) and (b)), the coarsening feature of the strengthening precipitates can be distinguished easily in the SZ at a low rotation speed (350 r/min). Under low welding heat input, welding heat input is insufficient for the dissolution of the strengthening precipitates, and the strengthening precipitates are coarsened. Increasing the rotation speed from 350 to 500 r/min is beneficial for providing more

heat input and dissolving coarsened strengthening precipitates. However, with high welding heat input (Figs. 1(c) and (d)), the coarsened strengthening precipitates are observed in the SZ at a low welding speed of 50 mm/min. Under high welding heat input, the heat input is enough to dissolve the strengthening precipitates. And the dissolved strengthening precipitates prefer to re-precipitate during FSW, and coarsen during cooling. A slow cooling speed (50 mm/min) leads to more re-precipitating particles coarsening than that at a high cooling speed (100 mm/min). It is clear that dissolution or coarsening of the initial particles in the SZ has occurred during FSW.

Figure 2 illustrates the TEM micrograph of SZ under P-PWNA−HT state, indicating that grains are not coarsened by the following artificial aging treatment. Comparing with the microstructures under PWNA state, more coarsened precipitates are detected in the joints welded at 350 r/min and 100 mm/min, 700 r/min and 100 mm/min, 500 r/min and 50 mm/min (Figs. 2(a), (c) and (d)). Figure 3 shows the detailed characterization of precipitates in SZ under P-PWNA−HT state. The rod-shaped particles are identified as T-phase (Al$_{20}$Cu$_2$Mn$_3$), which can remain during FSW because of its high dissolution temperature. The round-shaped particles which are rich in Al and Cu atoms are identified as θ-phase (Al$_2$Cu). Needle-shaped particles are observed in 500/100, 700/100, 500/50 samples (Figs. 3(b), (c) and (d)) and the selected area diffraction patterns (SADP) verify that these particles are $S(S')$ phase (Al$_2$CuMg or its metastable phase). No SADP of Guinier−Preston (GP) zones are detected, indicating that
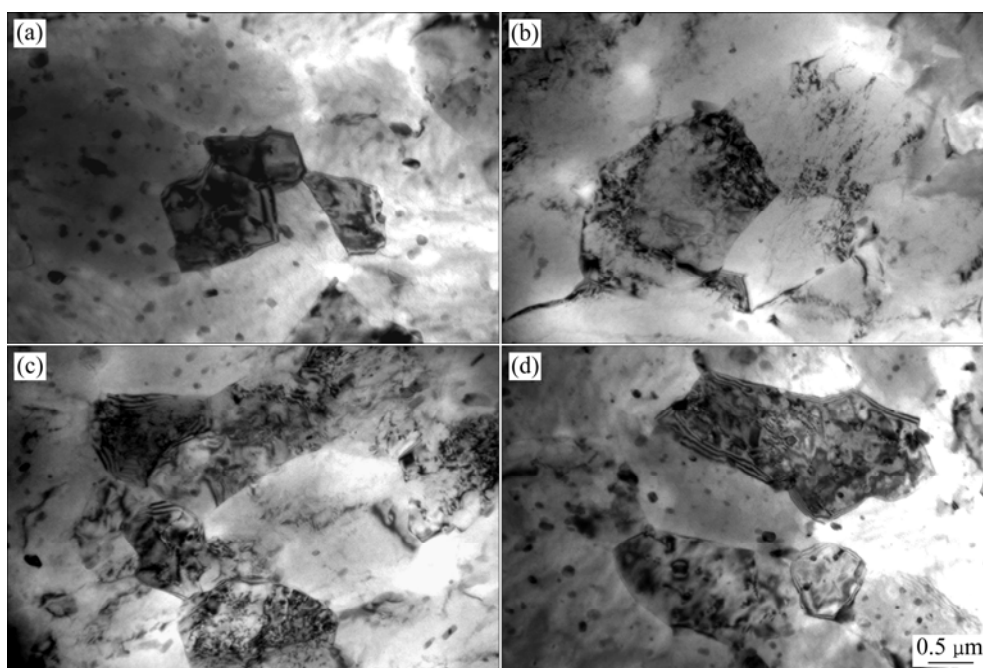

Fig. 1 TEM micrographs of SZ under PWNA state: (a) 350 r/min, 100 mm/min; (b) 500 r/min, 100 mm/min; (c) 700 r/min, 100 mm/min; (d) 500 r/min, 50 mm/min
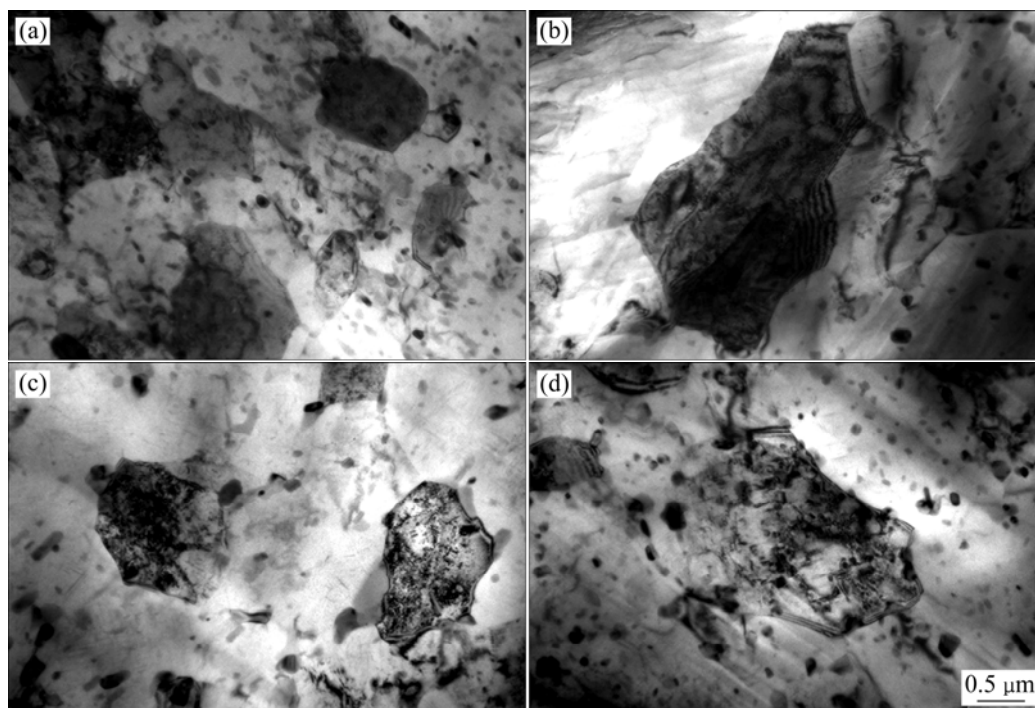
Fig. 2 TEM micrographs of SZ under P-PWNA−HT state: (a) 350 r/min, 100 mm/min; (b) 500 r/min, 100 mm/min; (c) 700 r/min, 100 mm/min; (d) 500 r/min, 50 mm/min
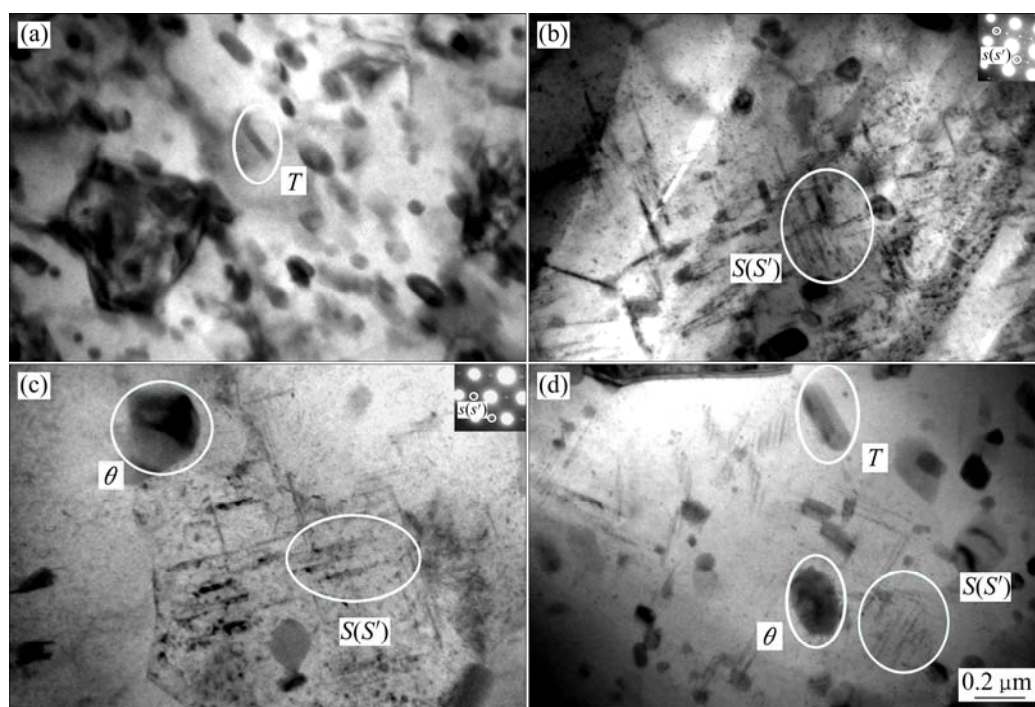

Fig. 3 Precipitates in SZ under P-PWNA−HT state: (a) 350 r/min, 100 mm/min; (b) 500 r/min, 100 mm/min; (c) 700 r/min, 100 mm/min; (d) 500 r/min, 50 mm/min

most of the GP zones have transformed to $S(S')$-phase. $S(S')$-phase is not stable above 190 °C, at which fine precipitates tend to coarsen. The coarsened $S(S')$-phase indicates that SZ under the P-PWNA−HT state has been overaged.

3.2 DSC analysis of strengthening precipitates

DSC analysis was conducted to further verify the types of the strengthening precipitates under both PWNA and P-PWNA−HT states. Figure 4(a) shows the result of DSC analysis of SZ under PWNA state at different

welding heat input conditions. In accordance with the 2024 aluminum equilibrium phase diagram, the formation temperature of the S(S′)-phase was around 280 °C. Therefore, the exothermic peak appeared at about 280 °C is attributed to the precipitation of S(S′)-phase. At temperatures lower than 280 °C, no obvious endothermic peak (dissolution peak of S(S′)-phase) is found, which indicates that the amount of S(S′)-phase in PWNA samples is small. It is known that the areas under the exothermic peaks of S(S′)-phase reflect the volume fraction of S(S′)-phase precipitated during DSC heating stage. The larger the area under the exothermic peak is, the more the substantial S(S′)-phase exists in the DSC specimen. The formation of S(S′)-phase is dependent on the consumption of the GP zones. The more the initial GP zones there are, the more the S(S′)-phase forms during DSC. Therefore, the volume fraction of S(S′)-phase precipitated also reflects the amount of the initial GP zones. The S(S′)-phase peak area of the 500/100 sample is the largest, indicating that the volume fraction of the GP zones in this PWNA joint is also the highest. The SZ containing a higher volume fraction of the GP zones can be attributed to the results of the welding heat input. Low welding heat input with a low rotation speed（350/100 sample）only coarsens the initial precipitates during FSW and high welding heat input (700/100 and 500/50 samples) coarsens the re-precipitating particles during cooling after FSW. The formation of coarsening precipitates decreases the amount of Mg and Cu atoms in the solid solution which are used to form GP zones during natural aging, thus reduces the amount of GP zones in the above three samples. Figure 4(b) shows the DSC analysis of SZ under P-PWNA−HT state, and no obvious endothermic or exothermic peak appears above 100 °C, indicating that GP zones have transformed to S(S′)-phase during P-PWNA−HT. Based on the results of DSC, it can be deduced that the strengthening precipitates in PWNA state are GP zones, while the ones in P-PWNA−HT state are S(S′)-phase.

3.3 Micro-hardness distribution

Figure 5 shows the micro-hardness distribution of the PWNA joints with different welding heat inputs and their corresponding joints after P-PWNA−HT. Under PWNA state, the hardness distribution in the 500/100 sample exhibits a "W" shape, while there is a "V" shape in other samples. A "V" shape indicates the minimum hardness value locates in the SZ. The different shapes of hardness distribution indicate that the hardness of SZ is sensitive to the welding heat input. With increasing the rotation speed, the average hardness of the SZ increases. At a rotation speed of 500 r/min and welding speed of 100 mm/min, the hardness of the SZ is nearly equal to
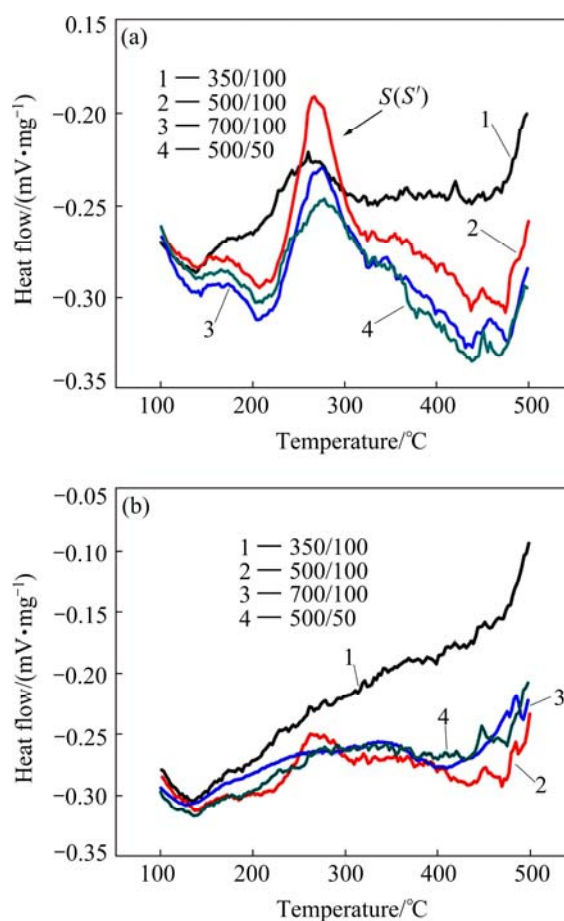

Fig. 4 DSC analysis of precipitates in SZ under PWNA (a) and P-PWNA−HT (b) states

that of the BM. However, the hardness decreases when the rotation speed is high (700 r/min). Furthermore, decreasing the welding speed reduces the hardness of SZ when the rotation speed is high (comparing with 700/100 and 500/50 samples). Therefore, it is difficult to describe the relationship between the rotation speed (or welding speed) and hardness, because both the rotation speed and the welding speed affect the hardness in SZ.

With aspect to the combined effects of the rotational and welding speed on the hardness of the SZ, the variations of the average hardness in the SZ under PWNA and P-PWNA−HT states with different welding heat inputs are shown in Fig. 6(a). In the range of low welding heat input condition, the average hardness in the SZ increases with increasing the welding heat input. The highest average hardness in the SZ is obtained at an LE/HI value of 5/2500, which corresponds to the weld parameters of 500 r/min and 100 mm/min. The rotation speed plays an important role in affecting the hardness of SZ where HI (which is mainly affected by the rotation speed) can represent the welding heat input accuracy under low welding heat input, but the average hardness in the SZ does not monotonously increase with increasing the welding heat input. Instead, under high
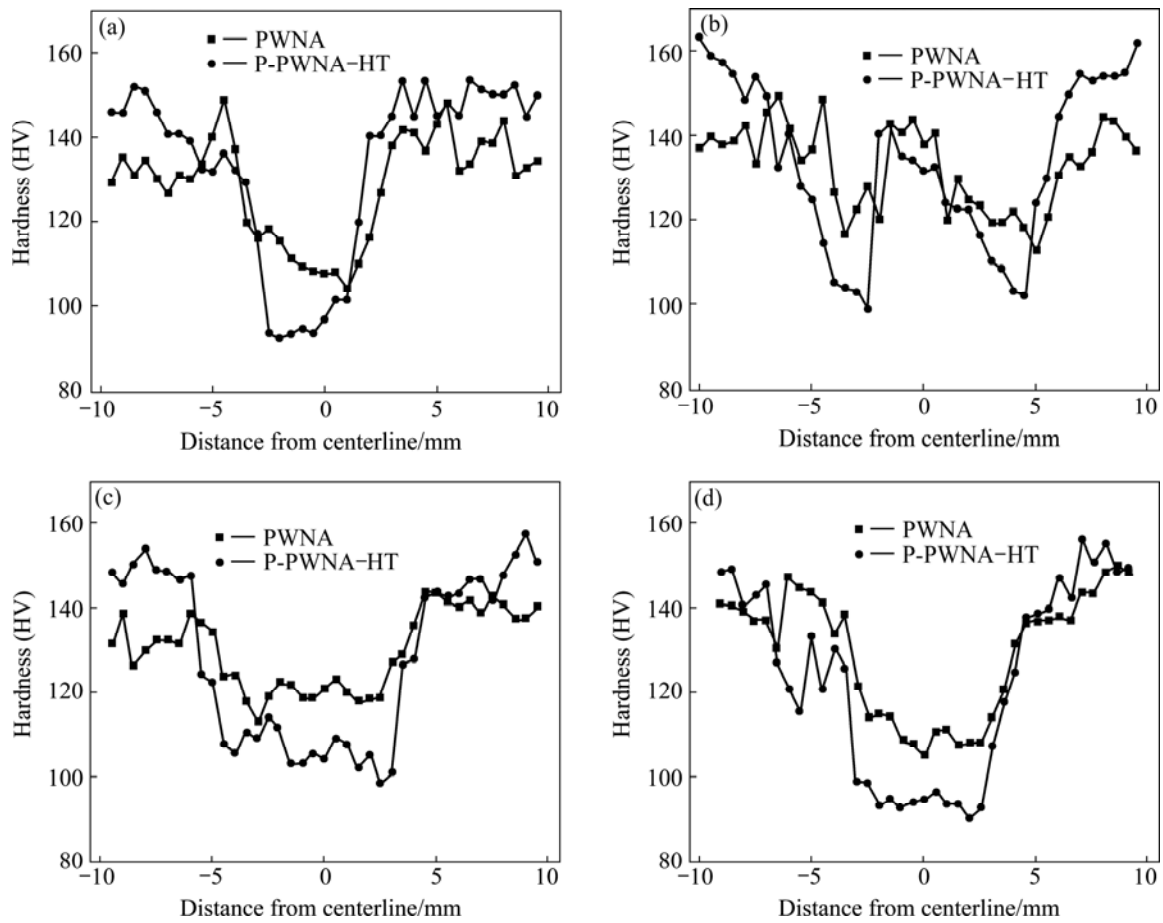
Fig. 5 Hardness distribution across cross-section of plates: (a) 350 r/min, 100 mm/min; (b) 500 r/min, 100 mm/min, (c) 700 r/min, 100 mm/min; (d) 500 r/min, 50 mm/min
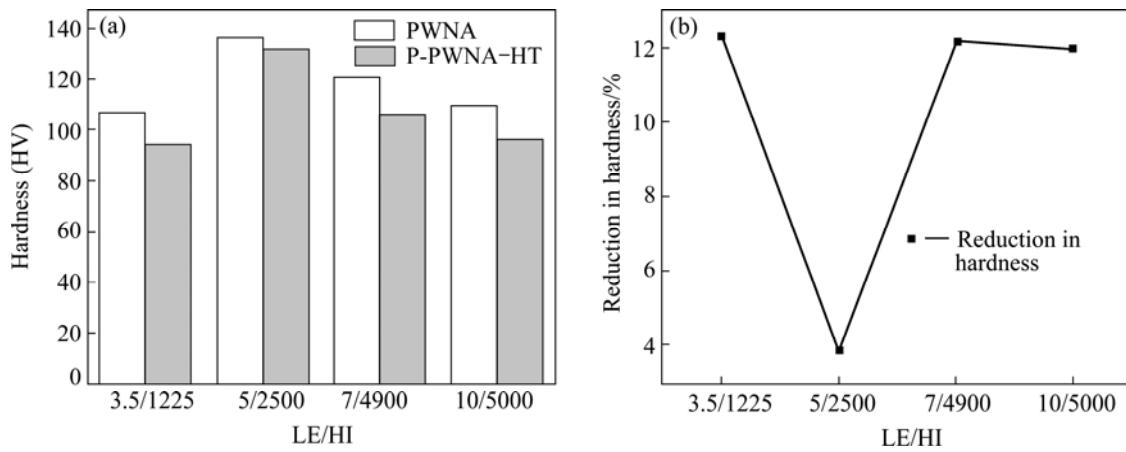

Fig. 6 Variation of average hardness in SZ (a) and reduction in hardness (b) under PWNA and P-PWNA−HT states

welding heat input condition, the average hardness decreases with increasing the welding heat input. It can be seen that the average hardness in the SZ drops to a lower level at high welding heat input (500/50 sample). Under the high welding heat input condition (500/50 and 700/100 samples), the difference in HI is only 100, but the hardness decreases by HV 12. However, the gap in HI is 2400 (500/100 and 700/100 samples) and the

hardness only decreases HV 16. This indicates that in the high welding heat input level, the effect of the welding speed on the hardness is more significant than that of rotation speed. And in this condition, the LE is more accurate than HI.

The hardness under P-PWNA−HT state is lower than that under PWNA state. The maximum reduction of the average hardness value (about HV 14) after

P-PWNA−HT occurs in the joint welded at 700 r/min and 100 mm/min. And Fig. 6(b) shows the variation of hardness between PWNA and P-PWNA−HT. The hardness in the joints is closely related to the distribution and morphology of the strengthening precipitates. During a long time heating at 220 °C, the samples under P-PWNA−HT state are overaged, and the coarsened $S(S')$-phase enhances the hardness limitedly, leading to a lower hardness than that of PWNA. However, because of the differences in the distribution and morphology of the strengthening precipitates under the PWNA state with different weld heat inputs, the response of the SZ to the P−PWNA−HT also differs. In the range with low welding heat input value, the reduction in hardness for 500/100 sample is the smallest (only about HV 4), indicating that high volume fractions of GP zones have a strong resistance to overaging. An optimal processing parameter is beneficial not only for avoiding the softening in SZ, but also for enhancing the resistance to overaging. Under other welding heat input, the resistance to overaging is low and the reduction in hardness is more than 10%.

4 Discussion

The microstructure in the SZ of the FSW joints undergoes intensive thermo-mechanical deformation, and there is an obvious grain refinement in the SZ because of the dynamic recrystallization processes. Grain refinement is an effective way to improve the mechanical properties of materials. However, in precipitation-hardened aluminum alloys, grain refinement is not the dominant strengthening mechanism. The hardness of a material is roughly proportional to the yield stress, and the relationship is the same as the Hall−Petch relationship:

$$H_v = H_0 + kd^{-1/2} \tag{5}$$

where H_v and k are the appropriate constants associated with the hardness measurements, and d is the grain size [26,27]. Based on Eq. (5), a large k is beneficial for improving the hardness. However, the value of k is relatively small in precipitation-hardened aluminum alloys [27], so that the effect of grain size on strengthening is not significant. The variations of hardness can be evaluated by the feature and the distribution of strengthening precipitates in the 2024 Al alloy.

In the typical precipitate evolution of 2024 alloy, metastable phases change from GP zones to S'-Al$_2$CuMg depends on the aging temperature. A well accepted sequence of transformation is as follows: supersaturated solid solution $\rightarrow$ GP zones $\rightarrow$ metastable S'-phase $\rightarrow$ stable S-phase [28−30]. In Ref. [28], the S'-phase was

described as a slightly strained version of the S-phase. Consequently, in the present work, the two phases of S and S' will not be distinguished. After FSW, the dissolved precipitates will be reserved in solid solution. With a 18 months−natural aging, the dissolved precipitates reform as GP zones, and it is difficult for $S(S')$-phase to form at room temperature. The properties of SZ under PWNA state depend greatly on GP zones. Figure 7 illustrates the relationship between the peak area of GP zones and the hardness under PWNA state. It can be seen that the volume fraction of GP zones, which is controlled by welding heat input, affects the properties significantly. Under the low heat input condition (350/100 sample), the precipitates cannot dissolve completely and the initial GP zones transform to $S(S')$-phase precipitates directly, decreasing the amount of GP zones during PWNA. Differently, the heat input of the 500/100 sample is sufficient for dissolving precipitates and limits coarsening of the particles. No coarsened $S(S')$-phase precipitates are detected in the 500/100 sample under PWNA state, as shown in Fig. 1(b). Therefore, the 500/100 sample shows high volume fraction of GP zones and excellent properties have been obtained under PWNA state. Under high welding heat input condition, GP zones dissolve completely, $S(S')$-phase precipitates reform and coarsen during FSW (Figs. 1(c) and (d)), which decrease the amount of the GP zones under PWNA state. Furthermore, a low welding speed reduces the cooling rate and leads to the formation of more coarsened $S(S')$-phase precipitates. This leads to a lower volume fraction of GP zones in the 500/50 sample relative to that in the 700/100 sample.
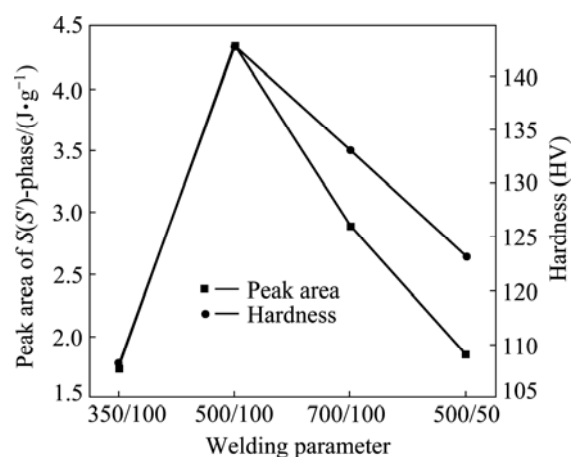

Fig. 7 Variation in DSC peak area and hardness with different welding parameters under PWNA state

Under P-PWNA−HT state, most of the GP zones are consumed by the formation of $S(S')$-phase. P-PWNA−HT is overaged, $S(S')$-phase coarsens, and the influence of GP zones can be neglected. The analysis of DSC (Fig. 4(b)) also shows the same result (no obvious

peak during heating).

Orowan−Ashby equation [21,27] is an effective method to evaluate the mechanical properties:

$$\Delta\sigma = \frac{0.13Gb}{\lambda}\ln\frac{r}{b} \tag{6}$$

where λ is the interparticle spacing, r is the particle radius, and b is the Burger vector (2.84×10^{-10} m for Al). This equation can be used to evaluate the hardness of aluminum alloy [31]. Based on Eq. (6), the effect of strengthening precipitates on mechanical properties in SZ is shown in Table 3. Under PWNA state, the volume fraction of GP zones in the 500/100 samples is the highest (Fig. 4(a)). A high volume fraction of GP zones is beneficial for increasing the amount of $S(S')$-phase. In Orowan−Ashby equation, r and λ are important parameters. A great amount of $S(S')$-phase can minimize λ. At the same temperature of heating, coarsening of the strengthening particles is limited, so the difference in r is small, which is the main reason that the 500/100 sample possesses excellent properties after P-PWNA−HT heat treatment. For other three parameters, coarsened $S(S')$-phase precipitates are found under PWNA state, and these precipitates coarsen further during heating, which limits the effect of precipitation strengthening.

Table 3 Effect of strengthening precipitates on mechanical properties in SZ under P-PWNA−HT state

ω/v	λ/nm	r/nm	$\Delta\sigma$/MPa	Hardness (HV)
350/100	165	103	34.29	94.15
500/100	75	72	71.37	131.78
700/100	113	85	48.44	105.99
500/50	142	97	39.43	96.12

5 Conclusions

1) The low-hardness zones of the FSW joints welded under different weld heat input conditions were all located in the FSW region. However, the average hardness in the SZ of the joint welded at 500 r/min and 100 mm/min reached a level nearly equal to that of BM at PWNA state.

2) The average hardness in the SZ was dependent on the rotation speed under a low welding heat input, and was on the welding speed under a high welding heat input. Under low welding heat input, HI was more accurate in calculating energy than LE, whereas LE was more suitable for high welding heat input.

3) After P-PWNA−HT, the average hardness in the SZ decreased because of overaging. However, the joint welded at 500 r/min and 100 mm/min showed a high resistance to overaging, and the reduction in hardness of SZ was less than 4%. An optimal welding heat input was

beneficial for elevating the resistance to overaging.

4) The grain refinement in the SZ had no significant effect on improving the hardness of the 2024 aluminum alloys. The morphology of the strengthening precipitates played an important role in the improvement of hardness distribution of the SZ. Higher volume fraction of GP zones avoided the softening in SZ. During the following heat treatment, sufficient amount of $S(S')$-phase formed from the GP zones to avoid the reduction in hardness.

References

[1] UDAY M B, FAUZI M N A, ZUHAILAWATI H, ISMAIL A. Advances in friction welding process: A review [J]. Science and Technology of Welding and Joining, 2010, 15(7): 534−539.

[2] NANDAN R, DEBROY T, BHADESHIA H K D H. Recent advances in friction-stir welding-process, weldment structure and properties [J]. Progress in Materials Science, 2008, 53: 980−986.

[3] CUI G R, MA Z Y, LI S X. The origin of non-uniform microstructure and its effects on the mechanical properties of a friction stir processed Al−Mg alloy [J]. Acta Materialia, 2009, 57: 5718−5729.

[4] CUI G R, MA Z Y, LI S X. Periodical plastic flow pattern in friction stir processed Al−Mg alloy [J]. Scripta Materialia, 2008, 58: 1082−1085.

[5] HAO H L, NI D R, HUANG H, WANG D, XIAO B L, NIE Z R, MA Z Y. Effect of welding parameters on microstructure and mechanical properties of friction stir welded Al−Mg−Er alloy [J]. Materials Science and Engineering A, 2013. 559: 889−896.

[6] REN S R, MA Z Y, CHEN L Q. Effect of welding parameters on tensile properties and fracture behavior of friction stir welded Al−Mg−Si alloy [J]. Scripta Materialia, 2007, 56: 69−72.

[7] BOUZAIENE H, REZGUI M A, AYADI M, ZGHAI A. Correlation between welding and hardening parameters of friction stir welded joints of 2017 aluminum alloy [J]. Transactions of Nonferrous Metals Society of China, 2012, 22(5): 1064−1072.

[8] JAYARAMAN M, BALASUBRAMANIAN V. Effect of process parameters on tensile strength of friction stir welded cast A356 aluminum alloy joints [J]. Transactions of Nonferrous Metals Society of China, 2013, 23(3): 605−615.

[9] KEIVANI R, BAGHERI B, SHARIFI F, KETABCHI M, ABBASI M. Effects of pin angle and preheating on temperature distribution during friction stir welding operation [J]. Transactions of Nonferrous Metals Society of China, 2013, 23(9): 2708−2713.

[10] DEHGHANI M, AKBARIMOUSAVI S A A, AMADEH A. Effects oc welding parameters and tool geometry on properties of 3003-H18 aluminum alloy to mild steel friction stir weld [J]. Transactions of Nonferrous Metals Society of China, 2013, 23(7): 1957−1965.

[11] JATA K V, SEMIATIN S L. Continuous dynamic recrystallization during friction stir welding of high strength aluminum alloys [J]. Scripta Materialia, 2000, 43: 743−749.

[12] GAN Wen-ying, ZHOU Zheng, ZHANG Hang, PENG Tao. Evolution of microstructure and hardness of aluminum after friction stir processing [J]. Transactions of Nonferrous Metals Society of China, 2014, 24(4): 975−981.

[13] SIVARAJ P, KANAGARAJAN D, BALASUBRAMANIAN V. Fatigue crack growth behaviour of friction stir welded AA7075-T651 aluminum alloy joints [J]. Transactions of Nonferrous Metals Society of China, 2014, 24(8): 2459−2467.

[14] SATO Y S, KOKAWA H, ENMOTO M, JOGAN S, HASHIMOTO T. Microstructural factors govening hardness in friction stir welds of solid-solution-hardened Al alloys [J]. Metallurgical and Materials

Transactions A, 2001, 32: 3033−3042.

[15] RAFI H K, RAM G D J, PHANIKUMAR G, RAO K P. Microstructure and tensile properties of friction welded aluminum alloy AA7075-T6 [J]. Materials and Design, 2010, 31: 2375−2380.

[16] XU W F, LIU J H, DONG C L. Microstructure and mechanical properties of friction stir welded joints in 2219-T6 aluminum alloy [J]. Materials and Design, 2009, 30: 3460−3467.

[17] LIU H J, FENG X L. Effect of post-processing heat treatment on microstructure and microhardness of water-submerged friction stir processed 2219-T6 aluminum alloy [J]. Materials and Design, 2013, 47: 101−105.

[18] LIU H J, ZHANG H J, YU L. Effect of welding speed on microstructures and mechanical properties of underwater friction stir welded 2219 aluminum alloy [J]. Materials and Design, 2011, 32: 1548−1553.

[19] HU Z L, YUAN S J, WANG X S, LIU G, HUANG Y X. Effect of post-weld heat treatment on the microstructure and plastic deformation behavior of friction stir welded 2024 [J]. Materials and Design, 2011, 32: 5055−5060.

[20] ELANGOVAN K, BALASUBRAMANIAN V. Influences of post-weld heat treatment on tensile properties of friction stir-welded AA6061 aluminum alloy joints [J]. Materials Characterization, 2008, 59: 1168−1177.

[21] AYDIN H, BAYRAM A, DURGUN I. The effect of post-weld heat treatment on the mechanical properties of 2024-T4 friction stir-welded joints [J]. Materials and Design, 2010, 31: 2568−2577.

[22] SHARMA C, DWIVEDI D K, KUMAR P. Effect of post weld heat treatments on microstructure and mechanical properties of friction stir welded joints of Al−Zn−Mg alloy AA7739 [J]. Materials and Design, 2013, 43: 134−143.

[23] SULLIVAN A, ROBSON J D. Microstructural properties of friction stir welded and post-weld heat-treated 7449 aluminum alloy thick plate [J]. Materials Science and Engineering A, 2008, 478: 351−360.

[24] DANAF E E, RAYES M E. Microstructure and mechanical properties of friction stir welded 6082AA in as welded and post weld heat treated conditions [J]. Materials and Design, 2013, 46: 561−572.

[25] FU R D, ZHANG J F, LI Y J, KANG J, HUI H J, ZHANG F C. Effect of welding heat input and post-welding natural aging on hardness of stir zone for friction stir-welded 2024-T3 aluminum alloy thin-sheet [J]. Materials Science and Engineering A, 2013, 559: 319−324.

[26] FENG X L, LIU H J, BABU S S. Effect of grain size refinement and precipitation reactions on strengthening in friction stir processed Al−Cu alloys [J]. Script Materialia, 2011, 65: 1057−1060.

[27] HANSEN N. Hall−Petch relation and boundary strengthening [J]. Scripta Materialia, 2004, 51: 801−806.

[28] CHARAI A, WALTHER T, ALFONSO C, ZAHRA A M. Coexistence of clusters, GPB zones, S''-, S'- and S-phases in an Al−0.9%Cu−1.4%Mg alloy [J]. Acta Materialia, 2000, 48: 2751−2764.

[29] RADMILOVIC V, KILAAS R, DAHMEN U, SHIFLET G J. Structure and morphology of S-phase precipitates in aluminum [J]. Acta Materialia, 1999, 47: 3987−3997.

[30] GENEVOIS C, DESCHAMPS A, DENQUIN A, COTTIGNIES B D, Quantitative investigation of precipitation and mechanical behaviour for AA2024 friction stir welds [J]. Acta Materialia, 2005, 53: 2447−2457.

[31] FENG X L, LIU H J, LIPPOLD J C. Microstructure characterization of the stir zone of submerged friction stir processed aluminum alloy 2219 [J]. Materials Characterization, 2013, 82: 97−102.

焊接热输入和焊后热处理对搅拌摩擦焊 2024-T3 铝合金焊核区硬度的影响

陈 雨[1]，丁 桦[1]，李继忠[2]，赵敬伟[3]，付明杰[2]，李晓华[2]

1. 东北大学 材料与冶金学院, 沈阳 110819；

2. 中国航空工业集团公司 北京航空制造工程研究所, 北京 100024；

3. School of Mechanical, Materials and Mechatronic Engineering, University of Wollongong, NSW 2522, Australia

摘　要：在不同焊接热输入条件下对 2024-T3 铝合金进行搅拌摩擦焊接，并利用透射电镜、差热分析和维氏硬度测试对焊核区的组织和硬度进行分析检测。研究表明，焊核区的硬度受到焊接热输入的影响。在高焊接热输入条件下，焊接速度的提升有利于提升焊核区硬度。而在低焊接热输入条件下，焊核区硬度随着旋转速度的增加而增加。焊后热处理导致组织过时效，焊核区硬度降低。相比于其他参数下获得的焊核区，旋转速度为 500 r/min，焊接速度为 100 mm/min 条件下获得的焊核区拥有较高的抗过时效性能，硬度下降仅为 3.8%，而其他焊核区的硬度下降超过 10%。焊核区硬度主要受到强化相形态的影响。

关键词：铝合金；搅拌摩擦焊接；热处理；热输入；硬度

(Edited by Yun-bin HE)